Semiconductor Optoelectronics
ISSN: 1001-5868

PERFORMANCE COMPARISON OF STAND-ALONE CNN AND HYBRID CNN MODEL FOR OSTEOARTHRITIS DETECTION

Sivaprasad Lebaka [1]*, Dr. D. G. Anand [2]
[1] Research Scholar, Department of Electronics and Communication Engineering, Visvesvaraya Technological University, Belagavi, Karnataka, India
[2] Rector - Research, Rajiv Gandhi Institute of Technology, Bengaluru, India

Abstract: Knee osteoarthritis (KOA) is the most frequent form of Osteoarthritis (OA) and is responsible for severe disability in individuals all over the world. One of the most severe types of arthritis is KOA. Knee replacement may be required if it is not addressed early. The most common approach to diagnosing KOA in clinical settings is still manual assessment, which entails segmenting knee joints and manually annotating the data, even though this is time-consuming and highly prone to human variation. Thus, several deep learning algorithms, particularly the Convolutional Neural Network (CNN), have been created to enhance the effectiveness of the clinical workflow in addressing the constraints of the generally utilized technique mentioned above. The data of knee thermal images is collected on its own. The collected images are then processed to change colors, get rid of noise, and improve quality. After image processing, the image is sent to a DL classification model after segmentation is performed. Three models, namely CNN, Hybrid Convolutional Neural Networks with Long Short-Term Memory (CNN-LSTM), and a CNN model combined with the Extreme Learning Machine (CNN-ELM), are used for DL classification. Three models were compared using criteria including accuracy, precision, recall, and F1-score, and the hybrid CNN-ELM emerged victorious in the automatic detection of KOA. The CNN-ELM achieves an accuracy of 94.33%.
Keywords: Osteoarthritis, Deep Learning, Accuracy, Hybrid Model, Convolutional Neural Network, Thermal Images

INTRODUCTION

OA is a common joint disease, and it is very expensive for both people and societies [1]. Late-stage OA symptoms include synovitis, bone anomalies, and cartilage degradation, the cause of which is unclear. The knee and hip are the most frequently affected joints by OA, with the knee being more commonly damaged than the hip [2]. The annual cost of OA for the world's roughly 250 million inhabitants is between 1% and 2% of GDP. KOA is on the rise as the global population ages [3]. Population-level analyses have found that gender, age, and Body Mass Index (BMI) are all related to OA. At least half of people over the age of 65 suffer from OA, and the risk increases sevenfold for those with a BMI of 30 or higher compared to those with a BMI of 25 or below. The financial burden of OA is substantial, both in terms of direct and indirect loss. OA is a prime example, costing hundreds of billions of dollars in the United States alone and ranking among Europe's top five reasons for annual healthcare spending [4]. A

clinical examination is currently the first step in diagnosing knee OA, with medical confirmation coming second. When the cartilage in a knee has deteriorated and a bone distortion has set in, the condition known as OA has set in. OA can be extremely painful and, in severe cases, render a person unable to move their knee at all. Total knee replacement (TKR) surgery is considered a "rescue procedure" for such a patient. Available data shows that the number of TKR procedures is high and rising [5]. Because of this, the number of TKR operations performed each year in the United States on patients aged 45 to 64 has increased by more than 100%. Therefore, it is essential to take worldwide precautions to avoid catastrophes. It is possible that imaging will help for the early identification of KOA symptoms, at which time changes in lifestyle (including exercise and diet) can slow or even stop the disease from progressing. Even in the earliest stages of the disease, anatomical alterations can be observed using imaging techniques like X-ray, ultrasound, MRI, and electron microscopy. Scientific studies have shown that the microcirculation of the surface skin can be affected by inflammation [6]. Physical changes may manifest externally as a result of the heat radiation released by diseased tissues and organs. Whether inflammation decreases or increases can affect the body's core temperature. Infrared thermography records these subtle temperature shifts, providing a non-subjective method for gauging the efficacy of treatments including medication, physical therapy, and surgery.

Thermography is a non-invasive, non-contact approach that uses a thermal imaging camera to visualize infrared radiation emanating from an object's surface. Taking thermal photos is a rapid, clean, and painless process that causes no harm to the subject. A correct picture of the temperature distribution can be obtained only by adhering to the method's requirements and suggestions [7]. Thermal vision techniques are helpful in medical examinations, and this is widely accepted. Medical applications of thermal vision technology include clinical drug testing, analysis of vascular reactivity in the hands, identification of Raynaud's syndrome, tracking of changes in OA, recognition of various forms of malignancies, and evaluation of diabetic foot skin health. Infrared imaging is employed in rheumatology to identify either increased or lowered temperatures, as a result of inflammation, nociceptive correlates, or vascular occlusion, respectively. This method can also be utilized in the detection of microcirculation, as well as the monitoring of temperature fluctuations caused by therapeutic interventions.

RELATED WORK

Recently many researchers focus on the automatic detection of OA from medical images due to its nature of affecting the large population in society. Some research articles from the year 2019 to 2023 are discussed in this section.

The research paper [8] provides a deep-learning model that can diagnose RA by analyzing thermal images. For this study, they scanned the palms of people with rheumatoid arthritis and a healthy control group to get thermal images of their hands. Then, the training is improved by subjecting the thermal pictures to pre-processing. To construct the deep learning model, employ a CNN-LSTM strategy. After training the model with thermal images, it can reliably predict the existence of rheumatoid arthritis. The results of both the training and the validation processes are documented. In addition, the data is graphically represented for ease of use. A strong correlation exists between the number of epochs and improvements in accuracy,

precision, and recall. There is a diminishing return on losses with time (known as an "epoch"). Once the model has been trained and validated, testing will yield values for each parameter. As the accuracy and precision values of this deep learning model have been significantly enhanced, it can be used as a screening tool for arthritis.

Using information about study participants' medical treatment and lifestyle choices, the author [9] trained a deep neural network (DNN) to identify cases of OA. A total of 5749 people took part in the research. Features were generated using Principal Component Analysis (PCA) with quantile transformer scaling using limited patient medical histories to identify cases of OA. By combining a DNN and scaled PCA, found that the suggested method could achieve an AUC of 76.8% with the least effort. So, this idea can be useful for both patients and doctors to use in preliminary screening for OA, lessening financial and time limitations. The use of ANNs and thermal image processing in MATLAB for early arthritis prediction is discussed in the journal [10]. Several stages make up the system. The thermal image will be loaded into the MATLAB Interface to initiate processing. The trouble spot can then be highlighted by clicking on it. Based on the pixel color in thermal images, the system will determine the temperature of the selected area. As inflammation occurs, white blood cells (WBC) release substances into the bloodstream. Redness and heat can be caused by the release of molecules that bring more blood to an injured or sick location. The temperature will be utilized as input in an early forecast using the Backpropagation method.

To aid doctors in the automatic detection of Knee OA on X-ray photographs, the authors of the article [11] describe a system based on deep learning techniques, employing the YOLO and VGG-16. They compile information, including X-ray images from the OAI's 2874-strong archive. Before being pre-processed using the CLAHE method, the data in this study were annotated and reviewed by chiropractors at Bach Mai Hospital. Finally, a pre-processed dataset is used to train the YOLOv3 model. An automated process then analyses the X-ray of the knee to pinpoint its precise location. When everything else fails, fall back on VGG-16's impressive categorization abilities. To further improve the problem's accuracy, use pre-processing approaches to boost image quality before training. The findings indicate that the suggested strategy is effective.

An adversarial evolving neural network (A-ENN) is proposed as a unique deep learning structure for measuring KOA severity in the study [12]. Convolution and deconvolution techniques allow ENN to effectively categorize the disease from light to extreme by evaluating an input image of varying KL grades. To record the traces of evolution, a discriminator-based adversarial training method is also created. To this end, they combine the general convolutional image descriptions with the evolutionary traces as a fine-grained knowledge base for longitudinal grading. It is important to keep in mind that ENN can be used in conjunction with already-existing deep architectures to learn extra tasks where the responses characterize progressive representations. Extensive experiments were conducted on the Osteoarthritis Initiative (OAI) dataset to determine the effectiveness of the suggested technique.

A novel learning approach is presented in the paper [13], which dynamically divides the OA dataset into two groups, one of which is more trustworthy than the other. To further aid CNN in its transition to both datasets, design a novel hybrid loss function. Using the proposed method, draw attention to typical samples while mitigating the impact of low-confidence situations. They compare two variants of an OA task and a five-class task using a five-way

split-plot design. Their technique gives better results than the traditional methods, with an average accuracy of 70.13%, on the OA assessment exam. The method outperforms, even though human assistance in the form of lesion location selection is still necessary for early-stage OA identification. Also, during the training phase, construct an experiment to evaluate the efficiency of large-scale autonomous data refinement. In light of this, they have only a shaky assurance that the sample descriptions are accurate. The OA Initiative generously provided the dataset utilized in this investigation.

In the journal [14], researchers detail how to use deep characteristics to spot KOA. This study, analyzed images to find out what factors lead to KOA using a CNN. The collected features are then used as inputs for several ML classifiers as the Support Vector Machine (SVM), K-Nearest Neighbour (KNN), and Naive Bayes (NB). This research used a classification system to classify images of KOA to better distinguish between the two types. The metrics over 90% utilizing several different assessment matrices show that the method works as intended in the testing results. The classification accuracy of the KNN-based deep features was higher than that of the SVM and NB.

The study [15] aims to establish a method for detecting OA in the hands by analyzing images, videos, and thermal data from one hundred patients at Keio University Hospital. Joint angles can be estimated from video footage using hand pose estimation, and those estimates can be utilized to build feature vectors. Joints in thermal and RGB images were taught to keypoint detectors so that they could be masked. The binary categorization of all joints is achieved by merging the recovered features and training them on SVM and CNN. In most cases, the proposed method has high accuracy and satisfactory F1 scores. They compare the individual and combined findings of each modality and find that video data, in addition to the combined method, yields the best outcomes. To identify OA, the suggested system combines optical and thermal data with ML, and early findings are encouraging.

The study [16] characterized a new ML-based computational strategy for autonomously monitoring swelling in RA by using hand thermography, a non-invasive imaging technique. Over four years, 595 patients with arthritis and osteitis diseases and healthy controls were enrolled in two hospitals. Using ultrasonography as the gold standard, hand thermal images were used to produce a thermographic inflammation rating, which provided a quantitative measure of joint inflammation. 449 individuals without rheumatic disease or with varying forms of arthritis were used to train and fine-tune the ML model. Analysis markers were used to gauge how well the approach performed with a validation set of 146 RA patients.

THEORETICAL BACKGROUND

To identify KOA from thermal images, the flow chart represented in figure 1 is followed. The data used to develop the DL model is collected by own using the thermal cameras. The collected real-time images are not suitable to train the DL model directly, some pre-processing is done on the data. Next to pre-processing, segmentation and classification are done to categorize the person whether affected by KOA or not. The theoretical concept of the segmentation and classification model are detailed in this section.

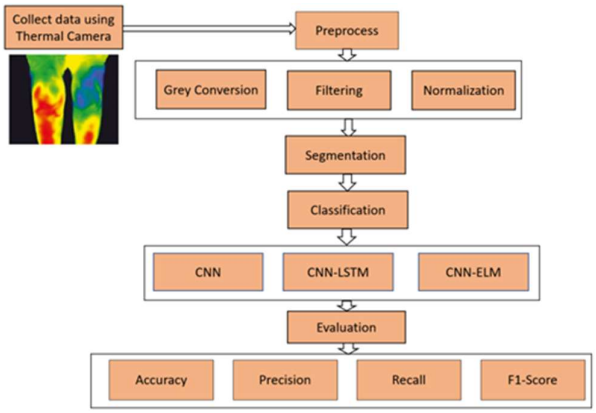

Figure. 1 Flowchart of the research work

3.1 Segmentation

To separate the warmest area (the white area) from the leg thermal images, we use a color-based k-means segmentation approach. This approach uses the least square error between the color pixel and the centroid and is rapid in computation and simple to apply. This article describes the suggested clustering algorithm.

Dorsal and ventral images of the legs were used to record the temperatures.

Two, the thermal image was transformed to the L*a*b color space [17], where L stands for brightness, a for red and green, and b for blue and yellow.

The proposed study selected and established the initial centres of five clusters (k = 5).

Calculate the distance from the leg's centre to each of the image's-colored pixels.

The minimum distance criterion was used to classify the data.

Cluster 1 separates the background

The red color area is separated by cluster 2

The green colour area is separated by cluster 3

The blue color area is separated by cluster 4

The white color (hot spot region) area is separated by cluster 5

The average of all L*a*b data was used to revise the five centroids.

Keep doing this until no more data move to a new cluster.

During the suggested research, no data are relocated to a new cluster when k is greater than 5.

This approach helps us to segment the leg region based on color or temperature. This pays the way for better classification of images using DL techniques.

3.2 Classification DL model

To classify the thermal images three different CNN models are employed such as conventional CNN, hybrid CNN like CNN-LSTM, and CNN-ELM. The construction and working of all three models are given below.

CNN: One of the most discriminative algorithms is CNN, which consists of layers of both convolutional layers (CL) and pooling layers (PL) [18]. Each successive layer is layered atop the previous one. The CL is accountable for the bulk of the layer's work, while the other layers reduce the CL's output and slow down the layer beneath it. The CNN has invariance properties as a result of the weight-sharing in the CL and the thoughtful selection of pooling algorithms. When it comes to image identification and computer vision, CNNs are among the best DL

vision approaches. In a CL of a CNN, feature maps are created by convolving a learnable kernel with the convolutional features mapping from the layer before it [19]. This kernel can have a non-linear or linear activation function (AF), and common examples include hyperbolic tangent, sigmoidal, and SoftMax. Hence, the results of each feature map are the sum of the results of many feature maps. Eq. (1) below demonstrates this:

$$x_j^i = f\left(\sum_{i \in M_j} x_i^{I-1} * k_{ij}^I + b_j^I\right) \quad [1]$$

where x_j^i → Outcome of the present layer; x_i^{I-1}→ Outcome of the pat layer; k_{ij}^I → Kernel of the current layer; b_j^I → Bias of the present layer. M_j → Input map selection. The PL requires a constant count of input and output feature map; when there are n input mapping, it requires approximately n output mapping [20]. In contrast, down-sampling shrinks every dimension of the resulting map to a smaller size. The technique can be stated mathematically as follows:

$$x_j^i = \text{down}(x_j^{I-1}) \quad [2]$$

When CNN is used to incorporate nonlinearity, the convolution, and pooling processes are not only used as their normal function but also as their AF.

CNN-LSTM: Recurrent neural networks (RNNs) have shown impressive outcomes on several tasks, notably forecasting, and classification [21], and one way to achieve this is by using long short-term memory (LSTM). By substituting memory components in the RNN's hidden units, the LSTM technique can pick up on long-term relationships [22]. It has been suggested to combine CNN-LSTM to bound the use of CNN to get the beneficial feature as well as ability with the higher efficiency of the LSTM method. This would make it easier to find and model short-term and long-term temporal relationships that are reflected in the order of the dataset. The hybrid CNN-LSTM comprises two pieces to accomplish this goal: 1) A one-dimensional CNN that performs the computational function on the input image and produces the features using CL and PL. 2) To make use of the features that were developed, LSTM and dense layers were used.

In the hybrid CNN-LSTM method, CNN is used for encoding while decoding is handled by LSTM. To feed information into decoding, an encoding must first acquire a feature from the input image it receives. Following this, the decoding isolates and models both the short and long-term temporal associations present in the given image.

Input layer: As input, the collected thermal image is provided.

CL-1: Uses the data from (i) as input and afterward adopts the outcomes to the feature maps.

CL-2: Utilizing 32 feature maps of each CL and a kernel size to enhance any features of interest.

Maximum PL: Oversimplifies the feature maps by removing specific features, resulting in a low-dimensional matrix.

Dropout layer: Enhances the model's protection from overfitting by way of improving the learning network.

Flatten layer: Converts the feature maps that were acquired into a single long vector

which may be utilized as input during decoding.

Vector layer: For every time step, the output sequence contains a copy of the underlying representation of the original input pattern.

LSTM Decoder: Features a hidden layer of 100 units that can produce the full arrangement, each of which contributes a normal allowance that can be used to anticipate what is the output.

Fully connected layer: Because they can interpret each step in the output prediction, LSTM decoders can behave similarly towards both output and fully connected layers at any one time.

Output layer: Declare whether the specified input contains KOA or not.

CNN-ELM: Using the MNIST dataset, the author of [23] illustrates and verifies the efficacy of a proposed Hybrid CNN-ELM. A CNN is composed of 3 layers: CL, the PL, and the SoftMax layer The CL, as its name suggests, requires convolving the input image using several kernels. CNN reliably generates multiple feature maps while conserving spatial context. Using a mean or maximum operation that is also spatially invariant, the PL helps to condense the feature map. Specifically, the feature extraction module consists of a CL and a PL. To accomplish this, this study will implement a CNN to extract features. The SoftMax AF is employed to categorize the input feature map in a SoftMax layer. The essential advantage of CNNs from fully linked networks that have the equivalent amount of hidden units is that they're easier to train. In the article [24], it is proposed that an ELM be used to train a Single Layer Feed-Forward Neural Network (SLFN). To reduce the need for constant fine-tuning, ELM's hidden layer nodes are seeded with random values before becoming fixed. The weights (or connections) between the hidden and output layer are the only free parameters. The SLFN training method used by ELM necessitates both a random feature mapping and a linear parameter solution.

This model relies on a voting ensemble where the majority vote determines the outcome. To begin, in a majority voting system, the total number of votes for each of the core classifiers is tallied. To make a prediction, a simple majority is used to decide which group it falls under. The prediction of the classifier receiving the most votes is used to make the final decision. An even number of characteristics is required for the simplest classifier. If a tie vote, the mode of operation is used [25]. To classify images, the study recommends utilizing a hybrid of CNN and ML models like SVM, NB, and KNN. Those CNN-ELM-based classifiers have been developed, each trained on a unique subset of the full dataset. The purpose of a CNN is to automatically learn and extract convolutional features from a train image collection. Multi-class classification is made easier with ELM thanks to its convolutional feature-based training. These three separate classifiers' results are then blended using a majority voting ensemble. Here is an explanation of the training approach taken for the proposed hybrid CNN-ELM systems:

INPUT: Training data [〖images:X〗_train, label:Y_train], Testing images 〖[X〗_test].

OUTPUT: Predicted label 〖[Y〗_pred]

PROCEDURE:

Split training data [X_train,Y_train] into N divisions

For every classifier C_i in N

Retrieving Convolutional Features from images of training data [〖images:X〗_train]

Train an ELM classifier [〖images:X〗_train, label:Y_train]

Determine the predicted class label Y_predi for the test data [〖images:X〗_test, label:Y_test]

End

To take a decision, a majority vote must be taken on Y_pred [Y_pred1,Y_pred2,….Y_predN].

Return Y_pred

RESULTS AND DISCUSSION

The purpose of this research is to use DL techniques, specifically hybrid, to detect arthritis present in infrared thermal images with high accuracy. This section details the steps involved from data collection to results obtained from developed DL models.

4.1 Data Collection

Reliable thermogram acquisition is aided by the establishment of a controlled environment and the adoption of a methodology that causes as little disruption as feasible. We created our OA-related dataset for this study using the proposed thermogram acquisition standard. Several acquisition-related parameters influence infrared thermogram analysis and consequently its evaluation [26]. The first stage in acquiring a thermogram image is to establish a secure environment to minimize the influence of confounding factors related to sensitivity. The quality of medical infrared thermograms is dependent on the capabilities of the thermal imaging camera used to take the pictures. The sensitivity and resolution of a camera influence its specifications. The high-resolution thermogram provides clearer, more detailed images, allowing for more exact analysis through image processing and a reduction in measurement errors. The FLIR T650sc thermal camera is used to capture thermograms for precise analysis and results. Temperature fluctuations of 0.02°C at 30°C can be monitored with an accuracy of ±1°C, or 1%, thanks to the system's great sensitivity.

When analyzing temperatures, the position of the camera matters. To take clear images, the separation between the thermal imaging camera and the target area has to be kept at less than 2m at all times. A camera with a tripod mount that allows for vertical height adjustment. Thermography becomes more precise when the camera and the target region are at a right angle to one another. The capture angle in pain thermography, on the other hand, may vary according to the target region. To obtain an accurate reading of the body's core temperature distribution, the thermogram must be taken under precisely regulated settings. Because external influences might alter thermography quality, it is critical to minimize environmental interference. The ambient temperature, humidity, and acquisition configuration are all critical factors. Temperature between 22°C to 25°C and relative humidity of 40 to 60% is recommended. Unnecessary artefacts in the thermogram could be caused by the emission of external infrared energy from sources like electric wires, pipelines, plugs, and so on. We made a black cloth to place behind the person to eliminate any unwanted artefacts [27]. The distance between the object and the thermal camera was used to determine the required background dimension.

4.2 Data Processing

First, we gathered reliable thermographic data of KOA and normal persons. Second, the thermal infrared images were pre-processed by converting the thermal image to a greyscale image and then refining the grey image to generate a distinct object border [28]. An average

filter was used to smooth the image, and a median filter was employed to eliminate the noise [29]. For image normalization, gamma correction was applied, which resulted in a significant improvement. These three strategies are interchangeable and can be used independently or in conjunction. To confirm the Gamma adjustment, the maximum image brightness histogram control was utilized [30].

4.3 Training Phase Outcome

The outcome of the CNN model on training and validation data is given in Figures 2 and 3. Figure 2 gives the accuracy plot of the CNN model over 50 epochs in both phases. The green is meant for training accuracy and the blue is for validation accuracy. The accuracy value of CNN will be 0.372 and 0.381 for the training and validation stage at the epoch of zero. As the number of epochs rises the accuracy value also gradually rises and attains a stable value in both stages after the epoch of 33. Finally, the accuracy reaches 0.798 in the training stage and 0.7812 in the validation stage. The loss plot of CNN over 50 epochs is given in figure 3. The same color as figure 2 will be used to differentiate both stages. The loss value starts at 1.0 and 0.82 in the training and validation phase at the zeroth epochs. And the final loss value attained by CNN will be 0.38 and 0.27.

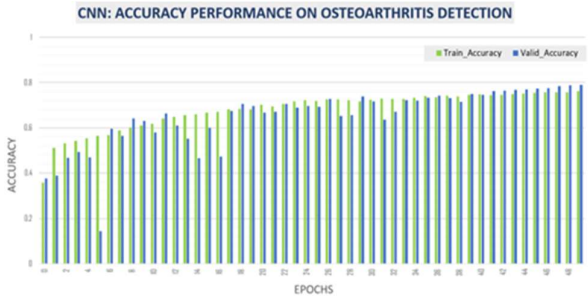

Figure. 2 Accuracy plot of CNN model

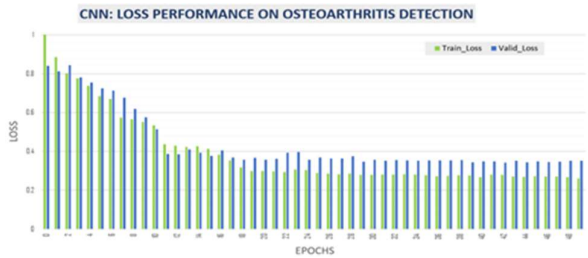

Figure. 3 Loss plot of CNN model

Figures 4 and 5 show the results of the CNN-LSTM model on the training and validation datasets, respectively. See Figure 4 for an accuracy plot of the CNN-LSTM model across 50 epochs, including the whole training and validating process. The blue bar represented a successful training session, while the red bar represented a successful validation. At the zeroth epoch, CNN-LSTM's accuracy values will be 0.398 and 0.391, respectively. After a period of 9 epochs, the values of accuracy for both phases are closer to 0.80. The ultimate training and validation accuracy is 0.841 and 0.824, correspondingly. Figure 5 displays the loss plot of CNN-LSTM over 50 epochs. In the training and validation phases, the loss value begins at 0.96 and 0.57. Moreover, the final loss value achieved by CNN-LSTM will be between 0.2 and 0.22.

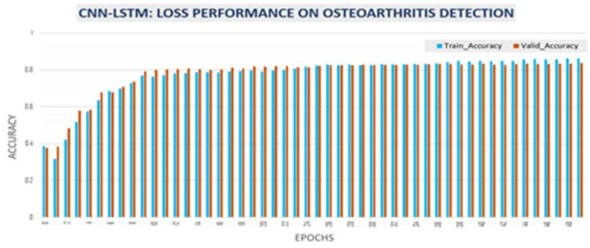

Figure. 4 Accuracy plot of CNN-LSTM model

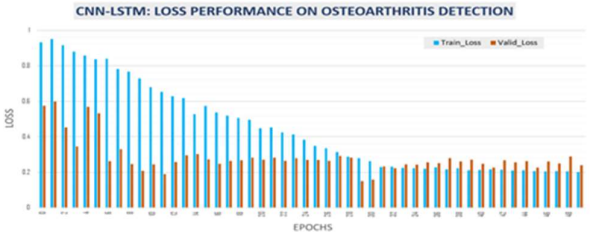

Figure. 5 Loss plot of CNN-LSTM model

The CNN-ELM model's performance on the training and validation datasets is depicted in Figures 6 and 7. If you look at Figure 6, you can see a representation of the CNN-ELM model's accuracy throughout 50 epochs, which includes the entire training and validation process. At the beginning and completion of the training, the accuracy values will be 0.784 and 0.987, correspondingly. The accuracy hits 0.8 immediately after the first epoch of training, and the same value is reached in validation by the 42nd epoch. A loss plot of CNN-ELM across 50 epochs is shown in Figure 7. At the beginning and completion of training, the loss value will be 1.0 and 0.583, and at validation, it will be 0.14 and 0.12. The blue and orange bars in both figures show the results of the training and validation, respectively.

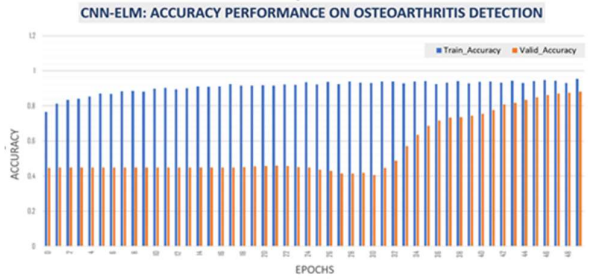

Figure. 6 Accuracy plot of CNN-ELM model

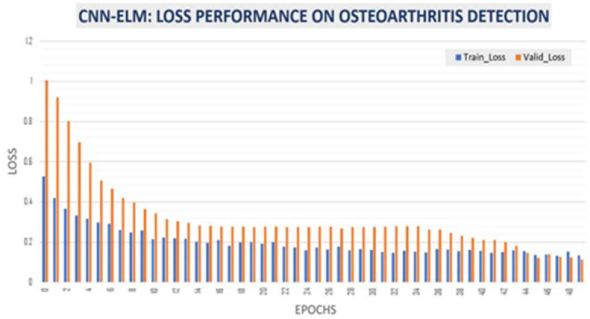

Figure. 7 Loss plot of CNN-ELM model

4.4 Testing Phase Outcome

The DL model architecture is finalized after the training and validation phase. Next, the finalized model is tested using the test data. The outcome of the three DL models on test data is evaluated using the metrics such as accuracy, precision, recall, and F1-score. The formula used to calculate those metrics is given below.

$$\text{Accuracy} = \frac{\text{TP+TN}}{\text{TP+TN+FP+F}} * 100 \quad [3]$$

$$\text{Recall} = \frac{\text{TP}}{\text{TP+FN}} * 100 \quad [4]$$

$$\text{Precision} = \frac{\text{TP}}{\text{FP+TP}} * 100 \quad [5]$$

$$\text{F1} - \text{score} = \frac{\text{2TP}}{\text{2TP+FP+FN}} * 100 \quad [6]$$

Figure 8 shows the comparison plot of the CNN, CNN-LSTM, and CNN-ELM models. All the metrics bars will be high for the CNN-ELM model when compared with CNN and CNN-LSTM. The hybrid CNN-ELM will give an accuracy of 94.33%, precision of 96.64%, recall of 92.30, and F1-score of 94.42% in the identification of OA.

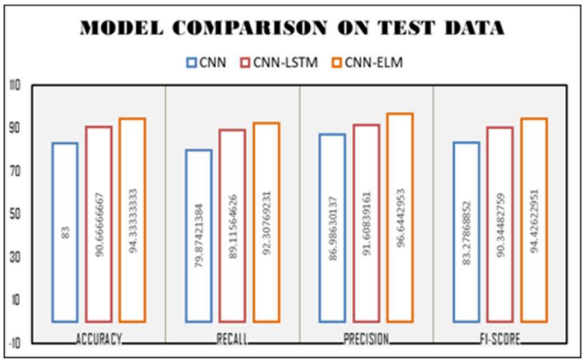

Figure. 8 DL model comparison on test data

CONCLUSION

For humans, KOA is a leading cause of physical disability. In rural places, where medical resources are scarce, people often don't find out they have KOA until it severely impairs their movement and treatment is challenging, making it too late to prevent permanent damage. When it comes to early detection, thermal images are used because they combine non-invasiveness, low cost, and widespread availability. According to studies of current methods, there is a need for enhancement in the accuracy of KOA identification. When given a sufficient amount of data for training, DL is predicted to improve accuracy. The use of an infrared camera allows us to produce our thermal data for this investigation. We then create three DL models, including CNN, CNN-LSTM, and CNN-ELM. The data was fed into the DL models for training and validation with epochs of 50. In both the training and validation phases, the model is assessed using accuracy and loss. Following this stage, the DL model is tested. A bar chart is used to visually compare the results from various DL models. When compared to the other two methods, CNN-ELM will produce more accurate predictions.

Conflicts of Interest

The authors declare no conflict of interest

Author Contributions

Both the authors involved in all phases of the research work and drafting of the paper.

REFERENCES

D. J. Hunter and S. Bierma-Zeinstra, “Osteoarthritis,” Lancet, vol. 393, no. 10182, pp. 1745–1759, Apr. 2019

Cross, Marita, Emma Smith, Damian Hoy, Sandra Nolte, Ilana Ackerman, Marlene Fransen, Lisa Bridgett et al. "The global burden of hip and knee osteoarthritis: estimates from the global burden of disease 2010 study." Annals of the rheumatic diseases 73, no. 7 (2014): 1323-1330.

Vos, Theo, Amanuel Alemu Abajobir, Kalkidan Hassen Abate, Cristiana Abbafati, Kaja M. Abbas, Foad Abd-Allah, Rizwan Suliankatchi Abdulkader et al. "Global, regional, and national incidence, prevalence, and years lived with disability for 328 diseases and injuries for 195 countries, 1990–2016: a systematic analysis for the Global Burden of Disease Study 2016." The Lancet 390, no. 10100 (2017): 1211-1259.

Mobasheri, Ali, and Mark Batt. "An update on the pathophysiology of osteoarthritis." Annals of physical and rehabilitation medicine 59, no. 5-6 (2016): 333-339.

Nguyen, Huy Hoang, Simo Saarakkala, Matthew B. Blaschko, and Aleksei Tiulpin. "Semixup: in-and out-of-manifold regularization for deep semi-supervised knee osteoarthritis severity grading from plain radiographs." IEEE Transactions on Medical Imaging 39, no. 12 (2020): 4346-4356.

Glik, Justyna, Armand Cholewka, Agata Stanek, Beata Englisz, Karolina Sieroń, Karolina Mikuś-Zagórska, Grzegorz Knefel, Mariusz Nowak, and Marek Kawecki. "Thermal imaging and planimetry evaluation of the results of chronic wounds treatment with hyperbaric oxygen therapy." (2019).

Ring, E. F. J., and Kurt Ammer. "Infrared thermal imaging in medicine." Physiological measurement 33, no. 3 (2012): R33.

Kumar, Dirisala J. Nagendra, K. Vidhya, S. Sagar Imambi, P. V. Pramila, Ashok Kumar, and V. Vijayabhaskar. "DL-based Rheumatoid Arthritis Prediction using Thermal Images." In 2022 Sixth International Conference on I-SMAC (IoT in Social, Mobile, Analytics and Cloud)(I-SMAC), pp. 1119-1124. IEEE, 2022.

Lim, Jihye, Jungyoon Kim, and Songhee Cheon. "A deep neural network-based method for early detection of osteoarthritis using statistical data." International journal of environmental research and public health 16, no. 7 (2019): 1281.

Wasnik, Swati, Vrishali Fulzele, Ishika Vora, Pankaj Khoabragade, Mrunal Raut and Md Waseem Khanooni. “Arthritis Prediction using Thermal Images and Neural Network.” International Research Journal of Engineering and Technology (IRJET) 07, (2020).

Huu, Phat Nguyen, Dat Nguyen Thanh, Thanh le Thi Hai, Hoang Chu Duc, Hung Pham Viet, and Cac Nguyen Trong. "Detection and Classification Knee Osteoarthritis Algorithm using YOLOv3 and VGG-16 Models." In 2022 7th National Scientific Conference on Applying New Technology in Green Buildings (ATiGB), pp. 31-36. IEEE, 2022.

Hu, Kun, Wenhua Wu, Wei Li, Milena Simic, Albert Zomaya, and Zhiyong Wang. "Adversarial Evolving Neural Network for Longitudinal Knee Osteoarthritis Prediction." IEEE Transactions on Medical Imaging 41, no. 11 (2022): 3207-3217.

Wang, Yifan, Zhaori Bi, Yuxue Xie, Tao Wu, Xuan Zeng, Shuang Chen, and Dian Zhou. "Learning From Highly Confident Samples for Automatic Knee Osteoarthritis Severity Assessment: Data From the Osteoarthritis Initiative." IEEE Journal of Biomedical and Health Informatics 26, no. 3 (2021): 1239-1250.

Zebari, Dilovan Asaad, Shereen Saleem Sadiq, and Dawlat Mustafa Sulaiman. "Knee Osteoarthritis Detection Using Deep Feature Based on Convolutional Neural Network." In 2022 International Conference on Computer Science and Software Engineering (CSASE), pp. 259-264. IEEE, 2022.

Guerreiro, Julian Jorge Andrade, Yoshimitsu Aoki, Shuntaro Saito, and Katsuya Suzuki. "Detection of Osteoarthritis from Multimodal Hand Data." In 2022 44th Annual International Conference of the IEEE Engineering in Medicine & Biology Society (EMBC), pp. 3607-3610. IEEE, 2022.

Morales-Ivorra, Isabel, Javier Narváez, Carmen Gómez-Vaquero, Carmen Moragues, Joan M. Nolla, José A. Narváez, and Manuel Alejandro Marín-López. "Assessment of inflammation in patients with rheumatoid arthritis using thermography and machine learning: a fast and automated technique." RMD open 8, no. 2 (2022): e002458.

Chitade, Anil Z., and S. K. Katiyar. "Colour based image segmentation using k-means clustering." International Journal of Engineering Science and Technology 2, no. 10 (2010): 5319-5325.

He, Kaiming, and Jian Sun. "Convolutional neural networks at constrained time cost." In Proceedings of the IEEE conference on computer vision and pattern recognition, pp. 5353-5360. 2015.

Alzubaidi, L. "Review of deep learning: concepts, CNN architectures, challenges, applications, future directions. J. Big Data 8 (1), 1–74 (2021)."

Algehyne, Ebrahem A., Muhammad Lawan Jibril, Naseh A. Algehainy, Osama Abdulaziz Alamri, and Abdullah K. Alzahrani. "Fuzzy neural network expert system with an improved Gini index random forest-based feature importance measure algorithm for early diagnosis of breast cancer in Saudi Arabia." Big Data and Cognitive Computing 6, no. 1 (2022): 13.

Yu, Yong, Xiaosheng Si, Changhua Hu, and Jianxun Zhang. "A review of recurrent neural networks: LSTM cells and network architectures." Neural computation 31, no. 7 (2019): 1235-1270.

Zhou, Bolei, Aditya Khosla, Agata Lapedriza, Aude Oliva, and Antonio Torralba. "Learning deep features for discriminative localization." In Proceedings of the IEEE conference on computer vision and pattern recognition, pp. 2921-2929. 2016.

Guo, Lili, and Shifei Ding. "A hybrid deep learning CNN-ELM model and its application in handwritten numeral recognition." Journal of Computational Information Systems 11, no. 7 (2015): 2673-2680.

Huang, Guang-Bin, Qin-Yu Zhu, and Chee-Kheong Siew. "Extreme learning machine: theory and applications." Neurocomputing 70, no. 1-3 (2006): 489-501.

Kannojia, Suresh Prasad, and Gaurav Jaiswal. "Ensemble of hybrid CNN-ELM model for image classification." In 2018 5th international conference on signal processing and integrated networks (SPIN), pp. 538-541. IEEE, 2018.

Zaproudina, Nina, Ville Varmavuo, Olavi Airaksinen, and Matti Närhi.

"Reproducibility of infrared thermography measurements in healthy individuals." Physiological measurement 29, no. 4 (2008): 515.

Denoble, Anna E., Norine Hall, Carl F. Pieper, and Virginia B. Kraus. "Patellar skin surface temperature by thermography reflects knee osteoarthritis severity." Clinical Medicine Insights: Arthritis and Musculoskeletal Disorders 3 (2010): CMAMD-S5916.

Dou, Mingsong, Chao Zhang, Pengwei Hao, and Jun Li. "Converting thermal infrared face images into normal gray-level images." In Computer Vision–ACCV 2007: 8th Asian Conference on Computer Vision, Tokyo, Japan, November 18-22, 2007, Proceedings, Part II 8, pp. 722-732. Springer Berlin Heidelberg, 2007.

Chang, Chin-Chen, Ju-Yuan Hsiao, and Chih-Ping Hsieh. "An adaptive median filter for image denoising." In 2008 Second international symposium on intelligent information technology application, vol. 2, pp. 346-350. IEEE, 2008.

Huang, Lihui, Gang Cao, and Lifang Yu. "Efficient contrast enhancement with truncated adaptive gamma correction." In 2016 9th International Congress on Image and Signal Processing, BioMedical Engineering and Informatics (CISP-BMEI), pp. 189-194. IEEE, 2016.